Synthesis of geopolymer using alkaline activation of building-related construction and demolition wastes

Synthesis of Geopolymer Using Alkaline Activation of Building-Related Construction and Demolition Wastes

Fan Gu[1], Jianwei Xie[1], Cedric Vuye[2], Ya Wu[3], and Junhui Zhang[1*]

[1] National Engineering Research Center of Highway Maintenance Technology, Changsha University of Science & Technology, Changsha, China

[2] SuPAR research group, University of Antwerp, Antwerp, Belgium

[3] Shenzhen Jianan Group, Shenzhen, China

* Corresponding author: zjhseu@163.com

Abstract

There are over 2 billion tons of building-related construction and demolition waste (brCDW) produced annually in China, but less than 30% of the waste is presently recycled. The majority of the brCDW is being disposed of in landfills in suburban or rural areas, resulting in a serious waste of resources and environmental pollution issues. This study proposed a high-value utilization approach for the brCDW, which was used as a precursor material to synthesize the high strength and environmentally friendly geopolymer. The brCDW was classified into three main components, namely, brick, ceramic, and concrete. The X-ray fluorescence (XRF), X-ray diffraction (XRD), particle size analyzer, and unconfined compressive strength tests were conducted to evaluate the influences of chemical composition and particle size of precursor materials on the strength of geopolymers derived from single and mixed brCDW components. The results demonstrated that the brick geopolymer exhibited a low strength in the early stage but a significantly high strength in the late stage. The ceramic geopolymer showed a low strength in both the early and late stages. The strength of concrete geopolymer was high in the early stage, but increased slowly later on. The mixed brCDW geopolymer had the highest early strength and the second-highest final strength compared to the single-component derived geopolymers. Furthermore, the XRD, scanning electron microscopy (SEM), and energy dispersive spectroscopy (EDS) tests were conducted to explore their microscopic mechanisms. The precursor materials dissolved in the geopolymerization process, thereby generating gels to coat and bind the unreacted particles. The formed gel type varied due to the different chemical composition ratios of precursor materials. The morphology and structure of brick geopolymer gels differed from other geopolymers, with the main gel products being C-A-S-H and N-A-S-H. The primary gel of ceramic, concrete, and mixed precursor geopolymers was the C-S-H gel, possibly with small amounts of C-A-S-H and N-A-S-H gel. Both the formed gel type and the compactness of the microstructure had significant influences on the geopolymer strength.

1 Introduction

With the rapid urbanization and infrastructure reconstruction, there are over 2 billion tons of building-related construction and demolition wastes (brCDW) produced annually in China, but less than 30% of the waste is presently recycled (Akhtar and Sarmah, 2021; Zhang et al. 2019; Zhang et al. 2020). The majority of the brCDW is being disposed of in landfills in suburban or rural areas, resulting in a serious waste of resources and environmental pollution issues (Zhang et al. 2019). Recently, the concept of a "zero-waste city" has been proposed to minimize the amount of produced waste and strengthen the recycling program. The Chinese Ministry of Ecology and Environment has also promoted this concept in more than 100 cities, aiming to improve the recycling rate of brCDW up to 60%. To achieve this goal, one potential solution is to develop a high-value utilization approach for the brCDW.

In road engineering, the recycled brCDW has been widely used as an alternative for subgrade filler or aggregates in asphalt mixture, cement concrete, granular base, and subbase (Zhang et al., 2019; Zhang et al., 2020; Hu et al., 2022; Tang et al., 2021; Guo et al., 2018; Bai et al., 2020; Chen et al., 2021). However, using the brCDW as a subgrade filler is a low-value approach, especially for the construction projects with heavy costs of material transportation. While using the brCDW as alternative aggregates improved its added value, the relevant implementation is limited due to the poor quality of the recycled aggregates. The existing studies were focused on the physical-chemical-biological modification of the recycled brCDW, but there was still lack of reliable technology to modify the brCDW for use in the upper layers of pavements (Mohammed et al., 2021; Peng et al., 2023; Mistri et al., 2020; Li et al., 2022; Feng et al., 2022; Tang et al., 2023). Geopolymer is a class of aluminosilicate materials with a three-dimensional structure ranging from an amorphous to semi-crystalline state. It is formed by polymerizing different types of aluminosilicate precursors through an activation process using alkaline activators (Davidovits, 1991). Compared to Portland cement, the production of geopolymer can approximately reduce carbon dioxide emissions by 40-60% and energy consumption by 60% (Gu et al., 2019; Barcelo et al., 2014; McLellan et al., 2011; Neupane, 2022). Additionally, geopolymer exhibits excellent engineering properties such as rapid setting, high strength, and high corrosion resistance (Vafaei et al., 2018; Aiken et al., 2018; Aliques-Granero et al., 2019; Lahoti et al., 2019; Shill et al., 2020; Obeng et al., 2023). The brCDW typically consists of brick, concrete, and ceramic, which contain large amounts of Si, Al, and Ca elements (Komnitsas et al., 2015). This indicates that the brCDW can serve as a suitable precursor for geopolymer, which will be a high-value and possibly environmentally friendly binder for construction materials.

80   The engineering performance of geopolymer is mainly dependent on the chemical
81 composition and particle size of precursor materials and the type and dosage of alkaline
82 activators (Komnitsas et al., 2015; Leong et al., 2016; Özbayrak et al., 2023; Jiang et
83 al., 2023; Jiang et al., 2023; Zhang et al., 2020). Fly ash, metakaolin, and slag are the
84 most commonly used precursor materials in geopolymer. The previous studies had
85 shown that the geopolymers derived from fly ash and metakaolin had an unconfined
86 compressive strength (UCS) ranging from 30 to 60 MPa after 28 days of curing, which
87 was comparable to that of cement concrete (Luna-Galiano et al., 2022; Temuujin et al.,
88 2010; Tchakouté et al., 2017; Chen et al., 2016). By using slag as a precursor material,
89 the geopolymer had even a higher UCS (i.e., 80 to 100 MPa) (Lemougna et al., 2020;
90 Komnitsas et al., 2009; Zhang et al., 2020). Due to the high residual alkalinity, many
91 types of industrial wastes such as red mud, coal gangue, and waste gypsum were also
92 used as a precursor material in geopolymer production. Although the geopolymers
93 derived from the industrial wastes had acceptable UCS, the leaching of heavy metals
94 from the geopolymers impeded their implementation (Nie et al., 2019; Yang et al., 2019;
95 Zhang et al., 2020).

96   In recent years, some pioneer researchers have used the brCDW as a precursor
97 material for geopolymer production. They found that the UCS of brCDW-derived
98 geopolymer had a wide variation, ranging from 10 MPa to 60 MPa (Sun et al., 2013;
99 Tan et al., 2022; Bassani et al., 2019; Hwang et al., 2019; Tuyan et al., 2018; Moreno-
100 Maroto et al., 2022; Xiao et al., 2022). This variability is attributed to the current
101 synthesis approaches, which do not adequately control the chemical composition and
102 particle size of brCDW. These factors may significantly impact the engineering
103 properties of geopolymer (Komnitsas et al., 2015; Petrakis et al., 2019; Ahmari et al.,
104 2012). The strength of the geopolymer is also influenced by the type and dosage of the
105 alkaline activator (Tchakouté et al., 2017; Kovtun et al., 2015; Helmy et al., 2016). The
106 most commonly used alkaline activators include sodium hydroxide solution and sodium
107 silicate solution. Many researchers had demonstrated that using a mixed alkaline
108 activator, rather than a single component, could significantly enhance the activation
109 effect, resulting in a higher strength of geopolymer (Ma et al., 2019). Note that
110 excessively high or low modulus (the mole ratio of SiO_2 to Na_2O) and dosage of
111 alkaline activators adversely affect the geopolymerization process and compromise the
112 quality of geopolymer. Thus, there is an optimal modulus and dosage for an alkaline
113 activator that achieves the highest strength of the geopolymer (Sivasakthi et al., 2021;
114 Ouyang et al., 2019; Luukkonen et al., 2020).

115   To address the aforementioned problems, this study aimed to develop an approach
116 for synthesizing a high strength geopolymer derived from the brCDW. The recycled
117 brCDW was classified into three components, namely, brick, ceramic, and concrete, for
118 analyzing the impact of the chemical composition of each component on the strength
119 of the geopolymer. Furthermore, this study evaluated the influences of the modulus and

dosage of the alkaline activator on the UCS of brCDW geopolymer, which was used to determine the optimal mix design for the geopolymers with single and mixed brCDW components. Finally, the microscopic mechanisms of brCDW geopolymer were revealed via the X-ray diffraction (XRD), scanning electron microscopy (SEM) and energy dispersive spectroscopy (EDS) tests (Gill et al., 2023).

2 Materials and test methods

2.1 Raw materials

The brCDW was collected from a local aggregate recycling plant, where the brCDW was pre-processed via crushing, separation, screening and stockpiling. In the laboratory, the brCDW with a particle size above 26.5 mm was cleaned by removing the debris such as plastic, metal and glass, and then dried overnight in an oven at 110°C. The processed brCDW consisted of 79% concrete, 16% brick and 5% ceramic in terms of weight proportion. To investigate the impact of the chemical composition of brCDW on the mechanical properties of the synthesized geopolymer, the brCDW was separated into concrete, brick and ceramic stockpiles. Sodium silicate and sodium hydroxide solutions were used as the alkaline activator. The sodium silicate solution was a transparent viscous liquid, composed of 27.3% SiO_2, 8.5% Na_2O, and 64.2% H_2O. The mole ratio of SiO_2 to Na_2O for sodium silicate was 3.3. The sodium hydroxide was a white flake solid with a purity level larger than 98%. The deionized water was used for diluting the alkaline activator solution. In this study, the diluted alkaline activator solution stood in the laboratory environment for 24 hours before use.

2.2 Preparation of precursor materials

To prepare the precursor materials, the recycled concrete, brick and ceramic were crushed, pulverized and ground, respectively. As shown in Figure 1, the recycled materials were crushed by a jaw crusher to a size range of 3-20 mm, and then pulverized by an ore mill to a size range of 100-600 μm. Finally, the pulverized materials were ground by a ball mill for a certain period of time. Since the particle size and uniformity of the precursor significantly affected the mechanical properties of geopolymer, this study aimed to assess the appropriate grinding time for the preparation of brCDW precursors. Thereby, four ball milling times (i.e., 2, 4, 6, and 8 hours) were selected to explore their impact on the particle size distribution of each precursor. The Mastersizer 3000 laser particle size analyzer was employed to determine the particle size distributions of the processed precursors.
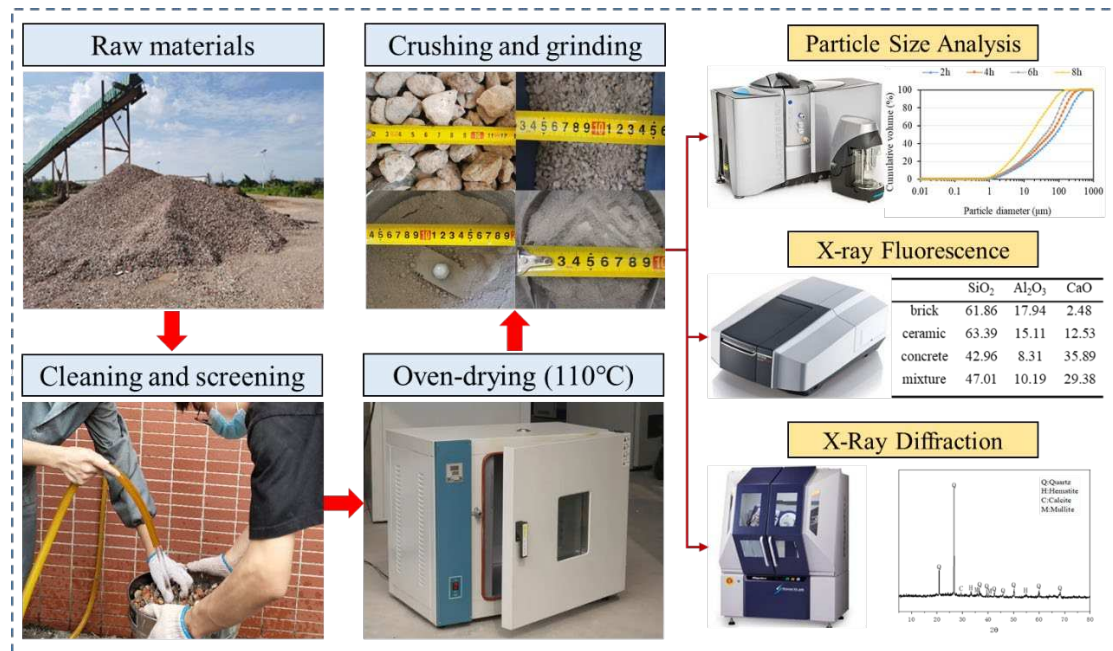
Figure 1. Pretreatment and research of Precursors
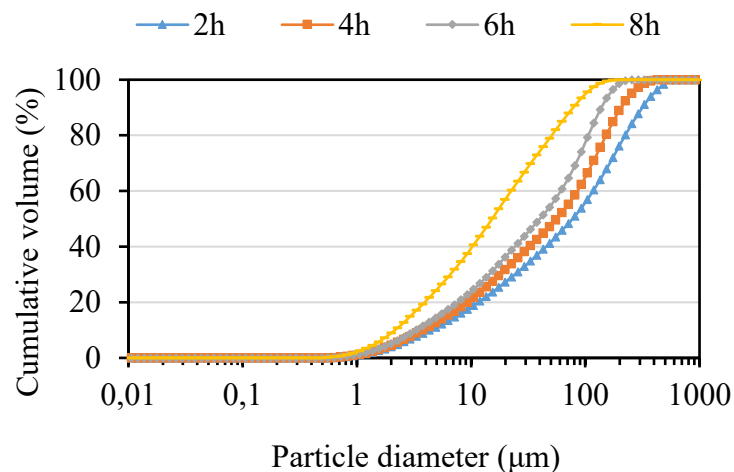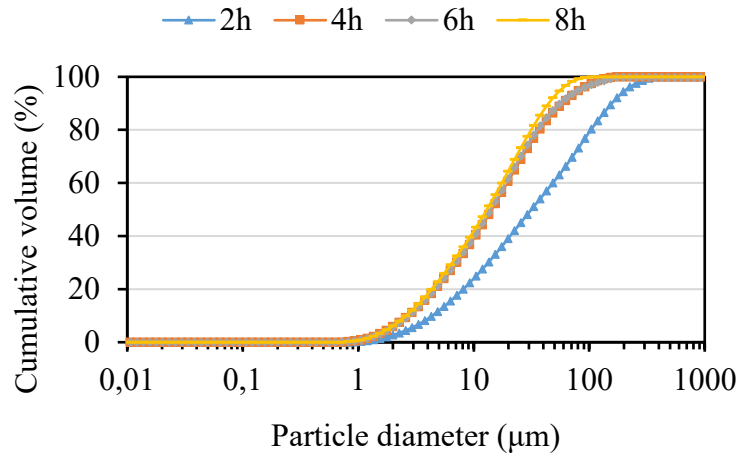
Figure 2 showed the particle size distributions of the processed concrete, brick and ceramic with different milling times. The median particle diameter (D50) was used to quantify the change in particle size of the precursor. As shown in Figure 3, the brick particle was much coarser than the ceramic and concrete particles after 2 hours of milling, and all the ground particles had a D50 smaller than 15 μm after 8 hours of milling.
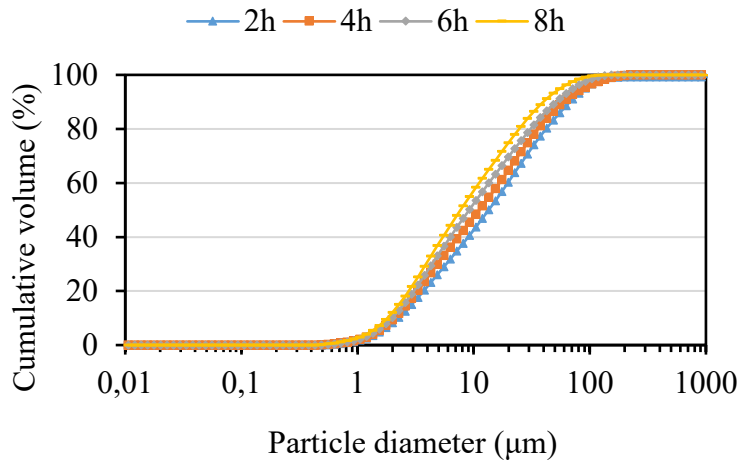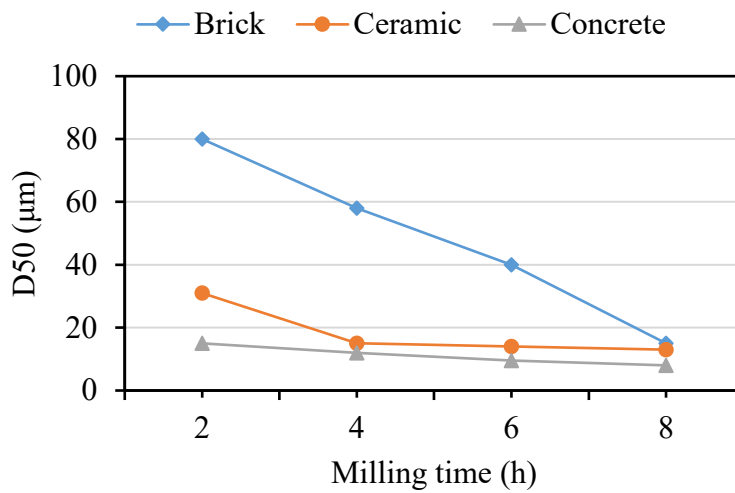

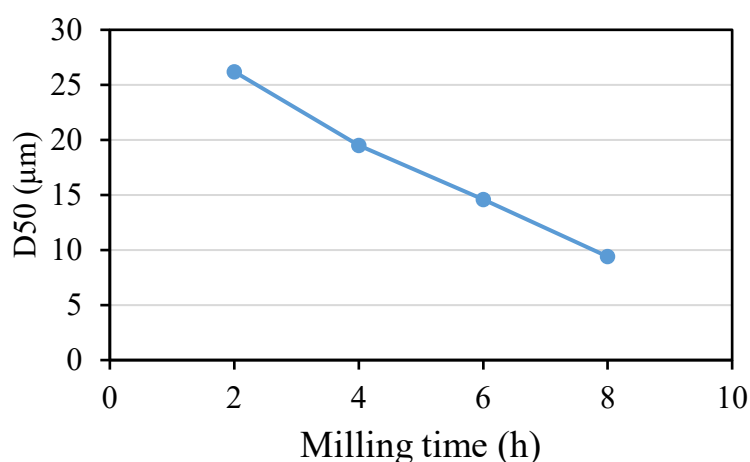**a. Brick precursor**

b. Ceramic precursor

c. Concrete precursor

Figure 2. Particle size distribution of brCDW

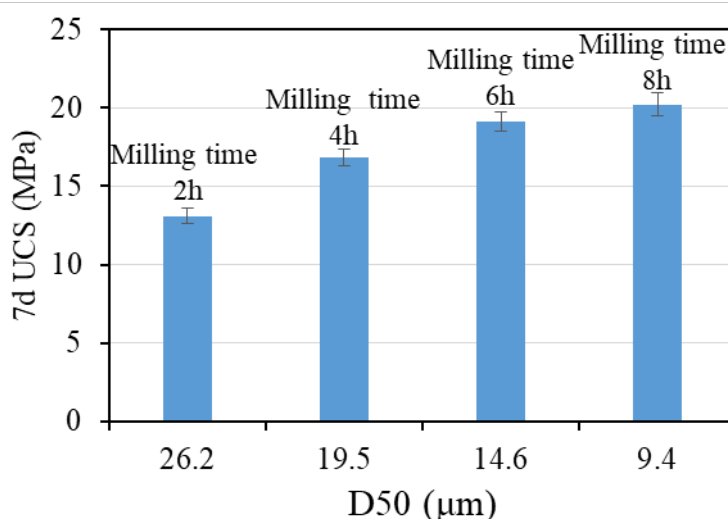**Figure 3. Relationship between D50 of brCDW and milling time**

172

Figure 4. Relationship between D50 of Mixed precursor and milling time

Figure 5. Relationship between UCS of geopolymer and D50

In general, a smaller particle size yields a larger specific surface area, which will increase the reaction rate between the brCDW and the alkaline activator (Petrakis et al., 2019; Ahmari et al., 2012). In order to explore the influence of particle size of precursor materials on geopolymer strength, the mixed precursor materials with different particle sizes were obtained after various milling times. According to the original proportion of each component in brCDW (brick: ceramic: concrete =16:5:79), the D50 of mixed precursor materials under different milling time was calculated using the weighted average method, as shown in Figure 4. The geopolymer was prepared with mixed precursors for 7-day UCS test. Herein, the modulus of the alkaline activator was 1.0, the dosage of the alkaline activator was 35%, and the water-precursor ratio was 0.35. Figure 5 presented the UCS test results. It was shown that the strength of the geopolymer was well correlated with the particle size of the precursor material. When the D50 of the precursor material was smaller than 15 μm, the change in the strength of

geopolymer became negligible. Therefore, by controlling the milling time, each precursor material was ground to a certain size with D50 equal to 15 μm.

2.3 Test methods

2.3.1 XRF test

The X-ray Fluorescence (XRF) test was performed via Shimadzu UV2700 fluorescence spectrometer under vacuum to determine the chemical composition of concrete, brick, ceramic and the mixed brCDW. The principle of XRF is to irradiate atoms with X-rays, causing the electrons of the irradiated atoms to undergo transitions and emit characteristic secondary X-rays. By testing and analyzing the characteristic radiation and its intensity for various elements, the types and concentrations of the elements can be determined.

2.3.2 XRD test

The mineralogical composition of concrete, brick, and ceramic brCDW was determined by XRD analysis. The diffraction patterns were obtained using a Rigaku Smartlab diffractometer equipped with Cu Kα 115 radiation, operating at 40 kV and 30 mA. The samples were scanned between 5° and 80° 2θ, with a step size of 0.02° 2θ and a scan rate of 4 °/min (Moreno-Maroto et al., 2022). The obtained diffraction data were analyzed using Jade software to establish the relationship between the angle and the strength of the test sample, thereby determining the phase composition of the materials.

2.3.3 UCS test

The UCS test was conducted by the YAW-300D microcomputer controlled pressure testing machine, with a loading rate of 2.4 kN/s. Prior to the test, the specimens were prepared with dimensions of 40 mm×40 mm×40 mm, and conditioned in a chamber with $20\pm2℃$ and 95% relative humidity for 7, 14 and 28 days. For the same condition, six replicates were prepared for unconfined compressive strength (UCS) testing.

2.3.4 SEM-EDS

The EVO-10 scanning electron microscope produced by Carl Zeiss was used for the experiments. Before the test, the selected samples were dried and cleaned using high-pressure blower to remove dust and other loose particles from the surface. The sample surface was plated with palladium before being fixed onto the sample table for imaging.

To identify the gel types in the different geopolymers, the EDS test was performed on the selected points of the geopolymer samples. This allowed for determination of the composition of the main elements in the gel. Note that the EDS test was conducted simultaneously with the SEM test using the same instrument.

226

## 3 Results and discussion

3.1 Chemical composition of brCDW

The XRF results were listed in Table 1. The chemical component of mixture was calculated based on the proportion of each component. The main oxides of each brCDW component were SiO_2, Al_2O_3, and CaO, which were the primary raw materials for geopolymer. Thus, the brCDW was highly suitable for geopolymer production. It was shown that SiO_2 always had the highest content, but its composition varied among the brCDW components. Brick had an extremely low CaO content but the highest Fe_2O_3 content, whereas ceramic had a relatively high CaO content but the lowest Fe_2O_3 content. Concrete had the highest amount of CaO, but a relatively low Al_2O_3 content. This was because the cement paste attached to the recycled concrete contained rich calcium and the limestone in the recycled concrete also provided calcium. Since the concrete was a dominant component in the brCDW, the chemical compositions of the mixed precursor were similar to those of concrete, which contained substantial amounts of SiO_2 and CaO.

Table 1. Main chemical components and contents of brCDW (%)

	SiO_2	Al_2O_3	CaO	Fe_2O_3	MgO	K_2O	TiO_2
brick	61.86	17.94	2.48	11.09	0.81	3.63	1.42
ceramic	63.39	15.11	12.53	2.72	1.40	3.03	0.62
concrete	42.96	8.31	35.89	5.71	1.24	2.61	0.73
mixture	47.01	10.19	29.38	6.42	1.18	2.79	0.84

Figure 6 showed the XRD patterns of each brCDW component. As presented, the brick mainly consisted of quartz, hematite, calcite, and mullite. The ceramic was primarily comprised of quartz, albite, and mullite. The main phases of concrete included quartz, calcite, albite, microcline, and muscovite. Since the mixed brCDW contained no new material, its primary phases included quartz, calcite, albite, microcline, and muscovite. Due to the low content of hematite in bricks and the fact that bricks only accounted for 16% of the mixed precursor, hematite was not detected in the XRD pattern of the mixed precursor. Thus, XRD may not be able to detect the phases with low content. The highest content in all materials was quartz, whose main component was SiO_2, as confirmed by the XRF test results. Furthermore, calcite in concrete was the main source of calcium, which was also proved by the XRF results. The brick and ceramic contained more aluminum elements that were primarily from mullite and albite. In addition, the high content of Fe_2O_3 in the brick may be mainly derived from hematite.
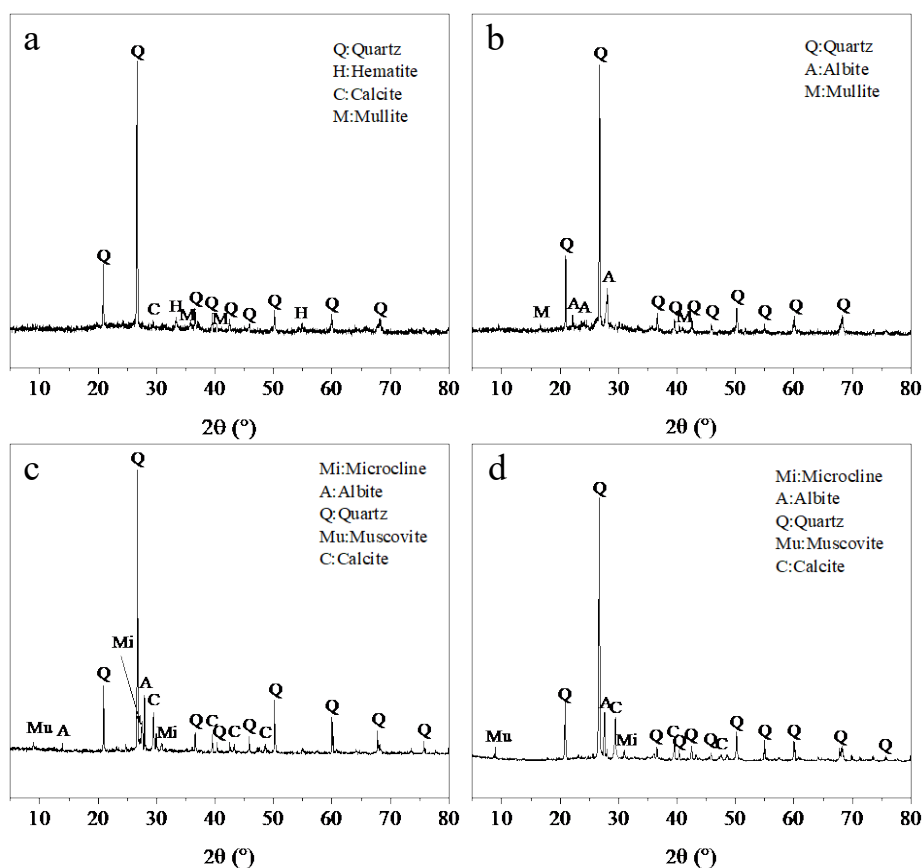
Figure 6. XRD pattern of brCDW: (a): brick, (b): ceramic, (c): concrete, (d): mixed precursor

3.2 Synthesis of geopolymer

3.2.1 Precursor material

To eliminate the influence of precursor particle size on geopolymer strength, it is important to control the particle size of the precursor materials since it greatly affects the reactivity rate. To achieve this, the D50 of each precursor material was controlled at 15μm by adjusting the milling time. The ball milling time for brick, ceramic and concrete was set at around 8 hours, 4 hours and 2 hours, respectively. Apart from preparing single-component geopolymer using each precursor material, the mixed-components geopolymer was also developed. Note that the mixed precursor followed the original proportion of each component of brCDW, with a specific ratio of brick: ceramic: concrete = 16: 5: 79.

3.2.2 Design of mix proportion

The alkaline activator's modulus can significantly impact the strength of geopolymer. To investigate this effect, it is necessary to adjust the modulus of the alkaline activator by adding sodium hydroxide. The initial modulus of the sodium silicate solution was 3.3. The relationship between the amount of sodium hydroxide (x)

276   to be added per 100 grams of sodium silicate solution and the target modulus of the
277   alkaline activator (M_x) was described by Equation 1.

$$M_x = \frac{m_s/M_s}{m_n/M_n + x/(2M_h)} \tag{1}$$

278   where M_x is the modulus of target activator; m_s is the mass proportion of SiO_2 in water
279   glass; M_s is the relative molecular weight of SiO_2; m_n is the mass proportion of Na_2O
280   in water glass; M_n is the relative molecular weight of Na_2O; M_h is the relative molecular
281   mass of NaOH.

282   The amount of alkaline activator was another crucial factor affecting the
283   strength of geopolymer. In this study, we referred to previous research and designed
284   three different dosages of alkaline activator (30%, 35% and 40%) for each modulus of
285   alkaline activator (1.0, 1.2 and 1.4) (Huo et al., 2021; Zhang et al., 2020; Luna-Galiano
286   et al., 2022), which was presented in Table 2. To ensure the proper fluidity of
287   geopolymer, we considered the water-precursor weight ratio as 0.35, based on the
288   findings from Huo et al. (2021).

289   **Table 2. Mix proportion of geopolymer**

Water-precursor weight ratio	Modulus of alkaline activator	Dosage of alkaline activator
0.35	1.0	30%
		35%
		40%
	1.2	30%
		35%
		40%
	1.4	30%
		35%
		40%

290

291   ***3.2.3 Production and curing***

292   The production of geopolymer was shown in Figure 7. Firstly, the required mass
293   of sodium hydroxide was calculated and added to the sodium silicate solution. The
294   resulting alkaline activator solution stood for 24 hours. Next, the precursor material was
295   mixed with the alkaline activator solution and stirred for 5-10 minutes. The geopolymer
296   slurry was poured into a mold in three layers and each layer was vibrated for 2 minutes
297   to remove air. The specimens were then covered with film to prevent water evaporation
298   and cured for 24 hours at room temperature. After that, the specimens were demolded
299   and placed in a constant temperature and humidity curing box for further curing
300   (Moreno-Maroto et al., 2022; Patil et al., 2014). The curing condition was $20 \pm 2 °C$

with 95% relative humidity. The specimens were tested at the designated curing time to assess their engineering properties. To ensure reliable results, each formulation yielded 18 cubic specimens (40mm×40mm×40mm), with six parallel specimens prepared for UCS test at each curing time.
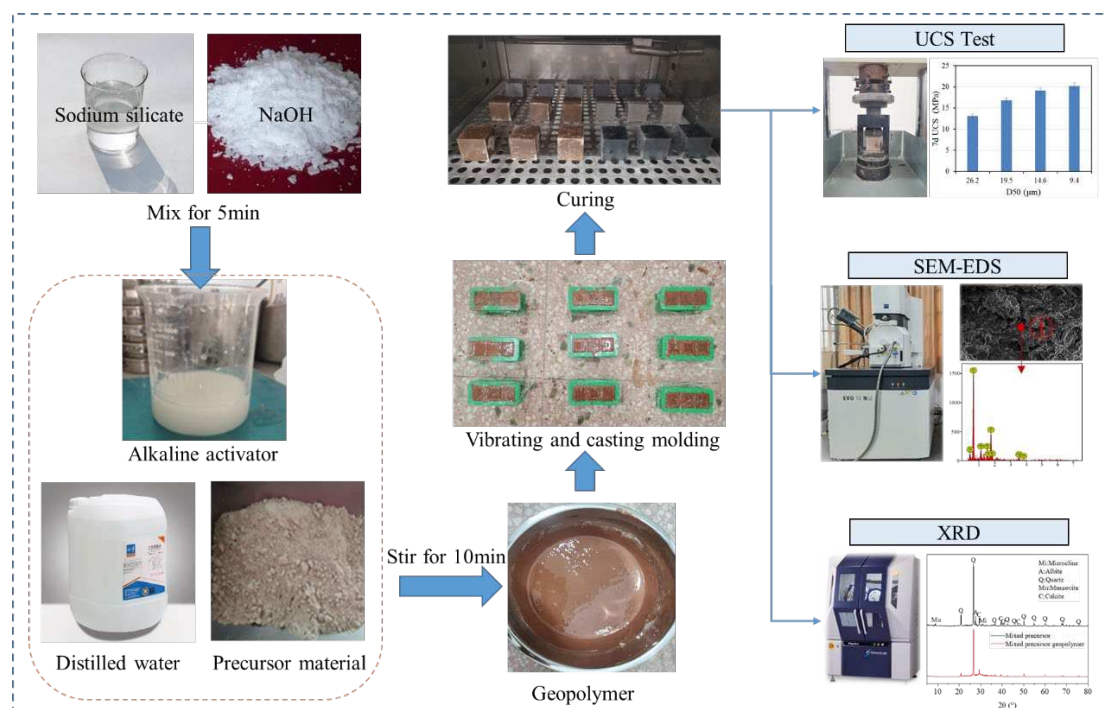
**Figure 7. Production and testing of geopolymer**

3.3 UCS test results

3.3.1 Geopolymer of brick precursor

Figure 8 presented the UCS of brick geopolymer. In this figure, 1.0, 1.2, and 1.4 represented the modulus of the alkaline activator and 30%, 35%, and 40% represented the dosage of the alkaline activator. A statistical analysis was conducted using the analysis of variance (ANOVA) with Tukey honestly significant difference test, with a confidence level set at 95% ($\alpha=0.05$). Labels A, A', A" were used to represent the group of samples with the statistically highest strength at 7, 14, and 28 days, respectively. Samples with different letters indicated a significant difference in strength, with lower alphabetical letters indicating lower strength grades.

The strength of brick geopolymer initially developed slowly, with a low UCS of only 2-8 MPa. However, the strength improved significantly in the later stage, with the highest strength of 29.9 MPa. There was no significant difference in the strength of the brick geopolymer prepared using the two mix proportions: a modulus of alkaline activator of 1.4 with a dosage of alkaline activator of 35% and 40%. However, the optimal mix proportion should have a lower alkali content, resulting in a more environmentally-friendly and cost-effective material for preparing brick geopolymer. Thus, a modulus of alkaline activator of 1.4 with a dosage of alkaline activator of 35%

was recommended as the optimal mix proportion. The low early-stage strength of brick geopolymer might be attributed to the low calcium content, which resulted in a low alkali consumption and generated only a small amount of C-S-H and C-A-H gels in the early stage. While the curing continued, most of the alkali reacted with the active silicon and aluminum components to form N-A-S-H and C-A-S-H gels, which provided the brick geopolymer high strength at the final stage.

The UCS of the brick geopolymer increased with the modulus of the alkaline activator, and the strength gain was greater with a lower modulus. For instance, the 28-day strength increased by an average of 6.8 MPa when the modulus increased from 1.0 to 1.2, but the average strength gain was only 3.7 MPa when the modulus increased from 1.2 to 1.4. This was likely because increasing the modulus of the alkaline activator improved the dissolution efficiency of active silicon, aluminum, and calcium components in precursor materials, particularly when the modulus was low. As the modulus of the alkaline activator increased, the dissolution efficiency of these components gradually decreased. When the modulus was 1.0 or 1.2, the strength of the brick geopolymer decreased with an increase in alkaline activator dosage, likely because the alkali content was high under these conditions. An excessive amount of alkali negatively affected geopolymerization, leading to a reduction in reaction products and structural damage.
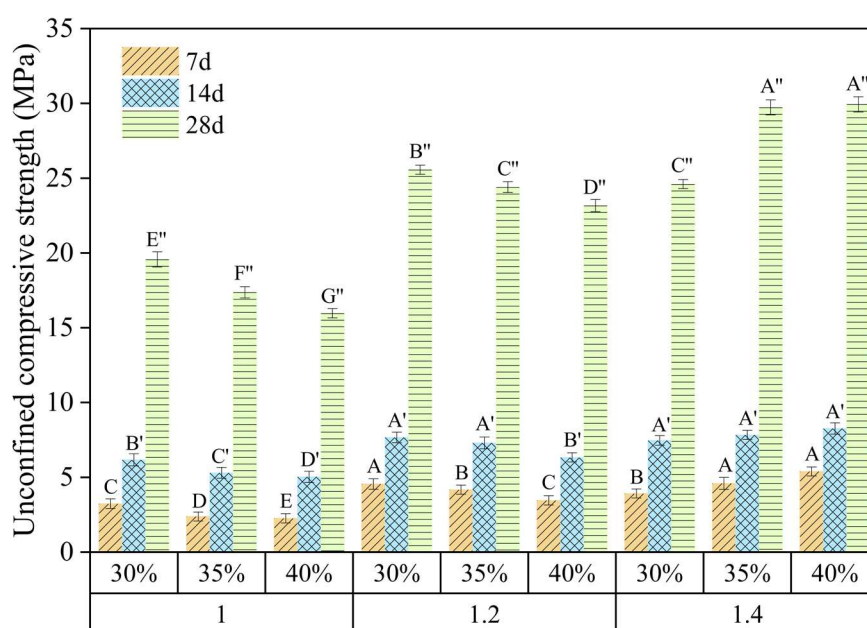
Figure 8. UCS of brick geopolymer

3.3.2 Geopolymer of ceramic precursor

Figure 9 showed the UCS of ceramic geopolymer. The 7-day UCS of ceramic geopolymer ranged from 6-9 MPa. Compared to the brick geopolymer, the early strength of ceramic geopolymer was generally higher. However, from 7 days to 14 days,

350 the strength only increased by 2-3 MPa. After 28 days of curing, the UCS only increased
351 by 1 MPa compared to the strength at 14 days. Ceramic geopolymer had lower strength
352 compared to other geopolymers and was not suitable for the production of high-strength
353 geopolymers. The reason for this phenomenon might be the calcium of the ceramic was
354 rapidly consumed by the alkaline activator at the early stage, and the geopolymer of
355 ceramic formed certain strength gels such as C-S-H and C-A-H. However, the calcium
356 of the ceramic consumed the alkaline activator and affected the progress of the
357 geopolymerization reaction, resulting in the formation of limited amounts of high-
358 strength geopolymer gels (N-A-S-H, C-A-S-H). Another reason could be the low
359 content of active silicon and aluminum components in ceramic, as most of these
360 components did not participate in the geopolymerization reaction. The highest strength
361 of ceramic geopolymer was observed when the modulus of the alkaline activator was
362 1.0 and the dosage of the alkaline activator was 35%, which was recommended as the
363 optimal mix proportion.

364   The UCS of ceramic geopolymer initially increased and then decreased with an
365 increase in the modulus of the alkaline activator. The strength of ceramic-based
366 geopolymer showed little increase when the modulus of the alkaline activator increased
367 from 1.0 to 1.2, but it decreased significantly when the modulus of the alkaline activator
368 increased from 1.2 to 1.4. For example, at 28 days, the UCS increased by an average of
369 0.9 MPa when the modulus of the alkaline activator increased from 1.0 to 1.2, while it
370 decreased by an average of 2.9 MPa when the modulus of the alkaline activator
371 increased from 1.2 to 1.4. This phenomenon may be attributed to the fact that most of
372 active silicon and aluminum components in ceramic dissolved efficiently at a modulus
373 of alkaline activator of 1.2. A further reduction in the modulus of the alkaline activator
374 did not significantly improve the dissolution efficiency and resulted in excess alkali.
375 The excess alkali affected the geopolymerization process and reduced the reaction
376 products. The remaining alkali also destroyed the formed gel structure, leading to a
377 reduction in geopolymer strength. When the modulus of the alkaline activator increased
378 from 1.2 to 1.4, the strength of the geopolymer decreased significantly because the
379 active silicon and aluminum components in the precursor materials could not dissolve
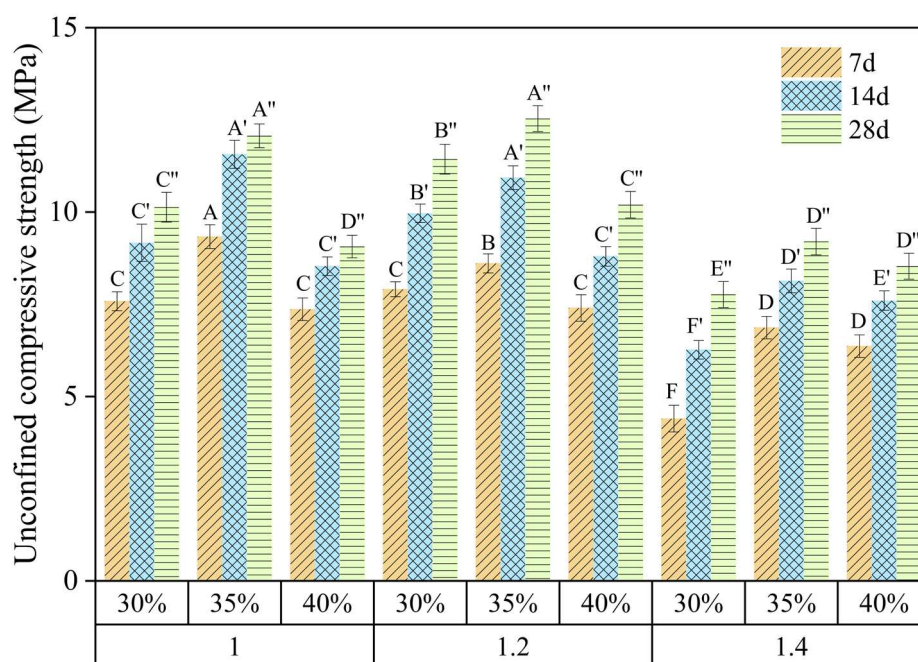380 fully due to the low alkali concentration.

Figure 9. UCS of ceramic geopolymer

3.3.3 Geopolymer of concrete precursor

As shown in Figure 10, the early-stage strength of concrete geopolymer exhibited rapid development and surpassed that of brick and ceramic geopolymer. However, the rate of strength development gradually slowed down in the later stages. The highest strength of concrete geopolymer was achieved when the modulus of the alkaline activator was 1.0 and the dosage of the alkaline activator was 40%, which was recommended as the optimal mix proportion. Note that this mix proportion had the highest alkali content. The abundance of calcium components in concrete necessitated a substantial amount of alkali for reaction. During the early stage, a larger quantity of gels such as C-S-H and C-A-H, were generated. In addition, a small amount of unhydrated cement particles could also undergo the hydration reaction. Consequently, concrete geopolymer exhibited significant early-stage strength. However, due to the high calcium content, a considerable amount of alkali was consumed, resulting in insufficient alkali for reaction with the active silicon and aluminum components in concrete, or a low content of active silicon and aluminum components. As a result, the formation of N-A-S-H and C-A-S-H gels was limited, leading to a slow strength growth in the later stage.

The UCS of concrete geopolymer decreased with an increase in the modulus of the alkaline activator at each stage. This phenomenon may be due to the fact that the active silicon and aluminum components in the concrete were fully dissolved when the modulus of the alkaline activator was 1.0, allowing the alkaline activator to react adequately with the precursor material. However, an increase in the modulus of the alkaline activator led to a decrease in alkali concentration, resulting in decreased

dissolution efficiency of the active silicon and aluminum components. Moreover, increasing the modulus of the alkaline activator led to insufficient geopolymerization and a reduction of reaction products, which ultimately lowered the geopolymer strength.
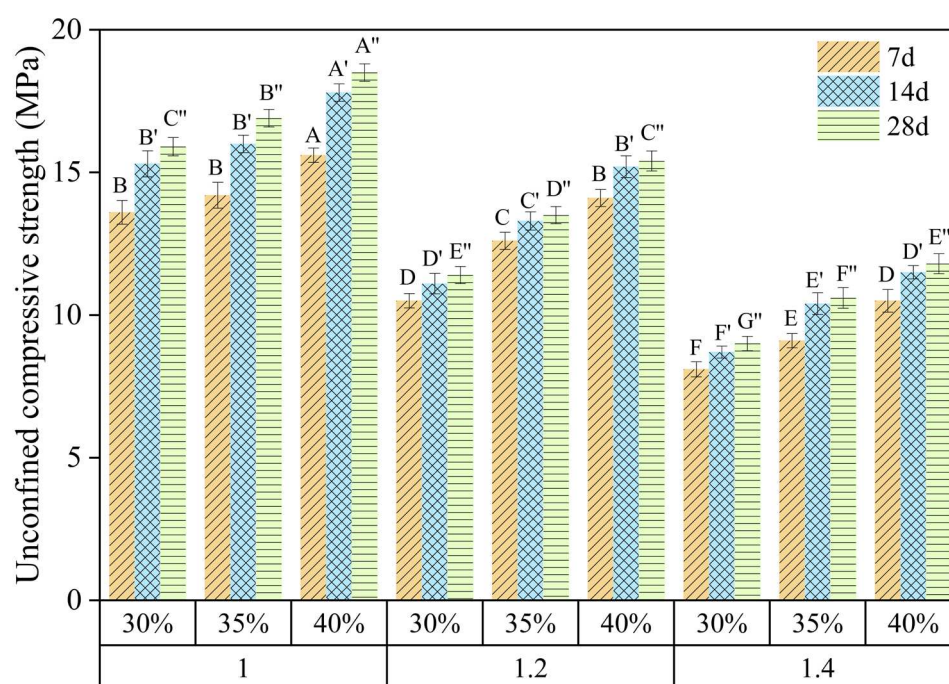

Figure 10. UCS of concrete geopolymer

3.3.4 Geopolymer of mixture precursor

Figure 11 showed the UCS of the mixed brCDW geopolymer. The strength growth of mixed brCDW geopolymer followed a similar trend to that of concrete geopolymer, and its early-stage strength of geopolymer was greater than that of brick, ceramic and concrete geopolymer. From 7 to 14 days, the UCS only increased by approximately 1-2 MPa, and from 14 to 28 days, the UCS only increased by around 1 MPa. The reason for this phenomenon may be that concrete accounted for 79% of the mixed precursor, with calcium comprising nearly 36% of it. The high calcium content results in the generation of a large amount of C-S-H and C-A-H in the early stage, leading to a rapid strength development. Furthermore, there may be unhydrated cement particles in the mixed precursor, which could undergo hydration reaction to provide additional strength. The mixed precursor also contained a small amount of brick and ceramic, which supplemented the silicon and aluminum components in the precursor materials, further enhancing the early strength of the mixed precursor geopolymer. However, the low content of brick and ceramic implied that the active silicon and aluminum components were not enough for an incomplete geopolymerization. Consequently, there was little formation of high-strength geopolymer gels (N-A-S-H, C-A-S-H) in the later stage, resulting in a slow strength growth.

429   The UCS of the mixed brCDW geopolymer decreased as the modulus of the

430   alkaline activator increased. This phenomenon may be due to the fact that when the

431   modulus of the alkaline activator was 1.0, the active silicon and aluminum components

432   in the mixed precursor were fully dissolved, resulting in the highest strength. Increasing

433   the modulus of the alkaline activator reduced the alkali concentration and the

434   dissolution efficiency of the active components, leading to an insufficient

435   geopolymerization and a lower geopolymer strength. For all moduli of alkaline

436   activator, the strength of the mixed precursor geopolymer increased with the increase

437   of alkaline activator dosage, and the strength of the mixed brCDW geopolymer was

438   highest when the modulus of alkaline activator was 1.0 and the dosage of alkaline

439   activator was 40%, which was recommended as the optimal mix proportion.
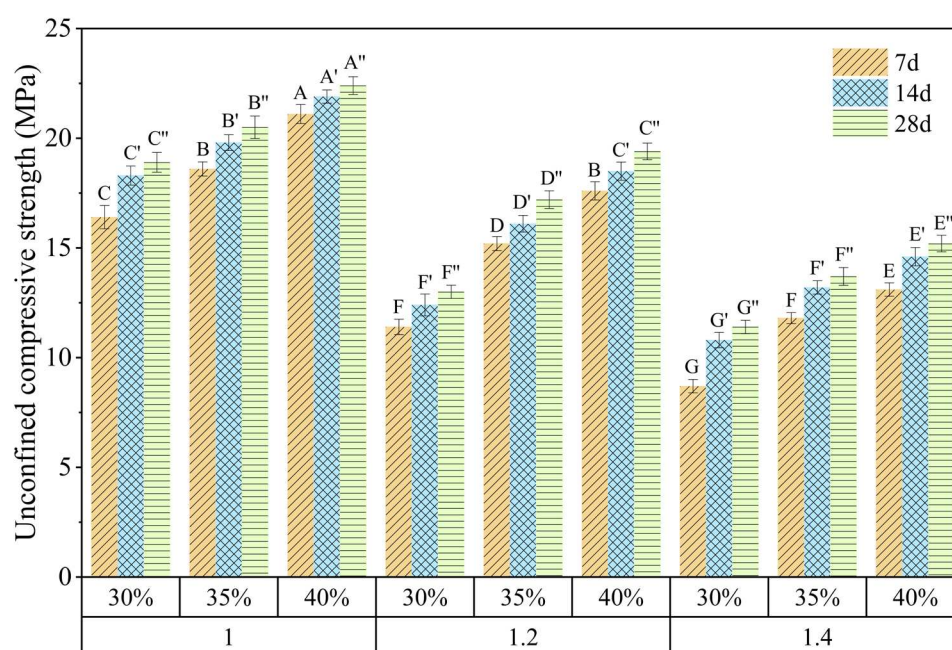
440

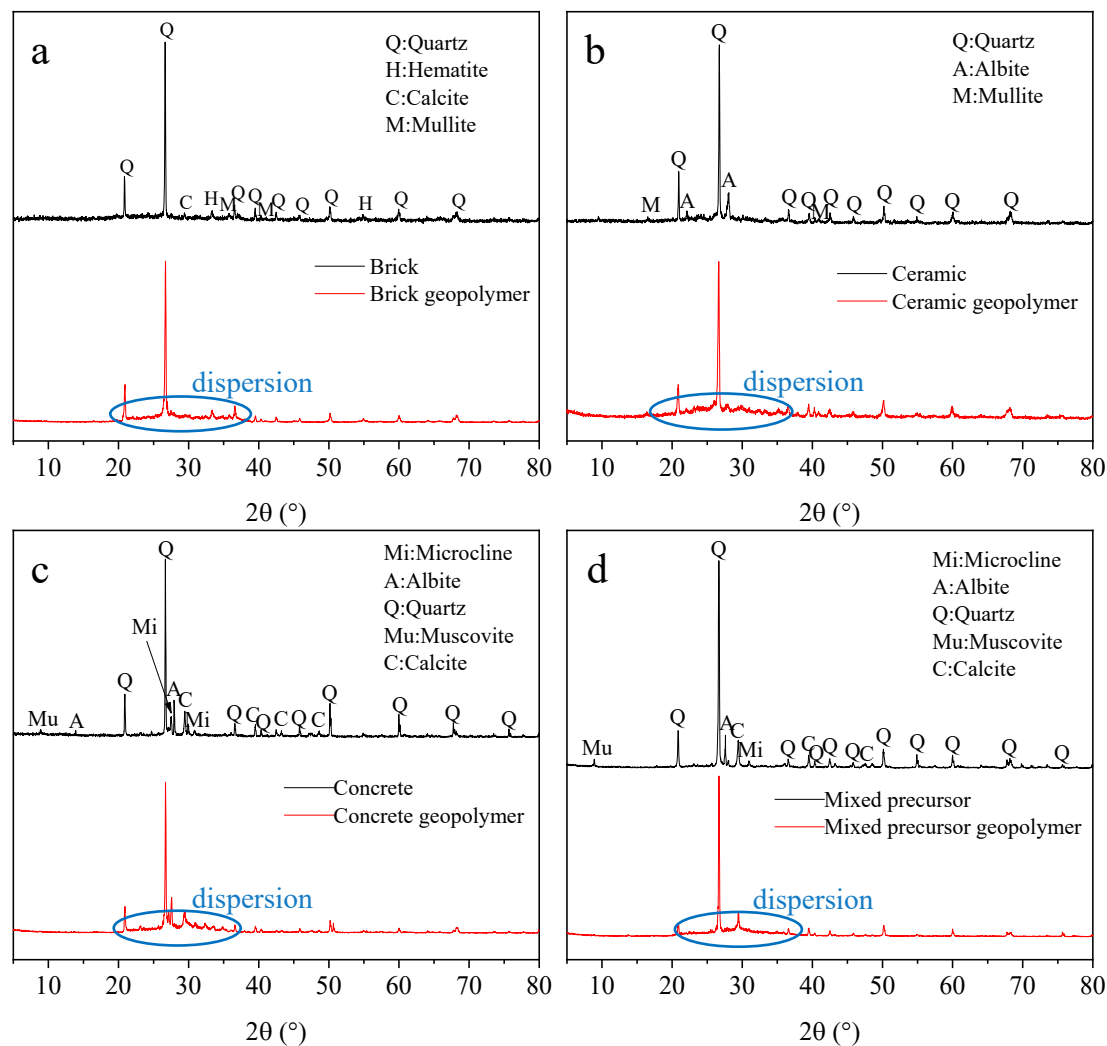441   **Figure 11. UCS of mixed precursor geopolymer**

442   *3.4 Microscopic mechanism of geopolymers*

443   *3.4.1 XRD test results*

444   In this section, we conducted the XRD test to analyze the phase composition of

445   brCDW precursor and geopolymer, which was then used to explore the changes in the

446   material phase before and after geopolymerization. Figure 12 presented the XRD

447   patterns of brCDW components and the derived geopolymers. The detected phases in

448   the geopolymers included quartz, muscovite, calcite, albite, and microcline, which were

449   originally present in the precursor materials, and no new phases were generated after

450   geopolymerization. Because geopolymer gels existed in an amorphous to semi-

451   crystalline state, there were no obvious crystallization peaks of reaction products in the

452   XRD pattern of geopolymer. Nevertheless, the XRD pattern of geopolymer showed a

453   dispersion peak at around 20°-40° 2θ, which was the characteristic peak of geopolymer

454 gels. Compared to the XRD pattern of the precursor material, an obvious change was
455 that the strength of partially crystallized peaks decreased, and some peaks disappeared
456 in the geopolymer pattern. This indicated that some phases dissolved and participated
457 in the geopolymerization, and other phases completely dissolved due to their low
458 content and participated in the reaction, causing their characteristic peak to disappear
459 in the XRD pattern of geopolymer.

460   The XRD patterns also demonstrated that the magnitude of the crystallization
461 peaks of the concrete and mixed precursors decreased most sharply. This suggested that
462 the amounts of dissolved and reactive substances in these materials were greater than
463 the other precursor materials. Additionally, the concrete geopolymer showed the most
464 distinct dispersion peak at 20°-40°2θ, indicating an abundance of gels. The significant
465 decrease in peak magnitude of calcite suggested that a large amount of calcium was
466 involved in the geopolymerization, and the resulting gels were primarily C-S-H and C-
467 A-H, which was confirmed in the EDS analysis later. In contrast, the XRD patterns of
468 ceramic and brick and their respective geopolymers showed a small decrease in peak
469 magnitude, indicating that fewer dissolved substances participated in the
470 geopolymerization. However, the brick geopolymer, despite having a smaller amount
471 of substances involved, had a more stable structure and higher strength than other
472 precursor materials.

Figure 12. XRD pattern of brCDW geopolymer: (a): brick geopolymer, (b): ceramic geopolymer, (c): concrete geopolymer, (d): mixed precursor geopolymer

3.4.2 SEM test results

We also performed the SEM test on the optimal mix proportion of brCDW geopolymers at 7 and 28 curing days for analyzing their microstructures. Figure 13 illustrated the microstructure of geopolymers, which is comprised of gels, unreacted particles, cracks, and pores. Since the brCDW had low activity, some particles did not dissolve and participate in the geopolymerization. Other precursor materials dissolved and reacted to form gels, which covered the unreacted particles and bound them together. The strength of the geopolymer was formed after the gel hardened. The pores and cracks had an adverse impact on the strength of the geopolymer. The formation of pores may be due to the presence of water and air in the geopolymer. As water and air dissipated, the space they occupied initially evolved into these pores. The cracks may have formed due to the loss of water in the geopolymer, resulting in a shrinkage issue.
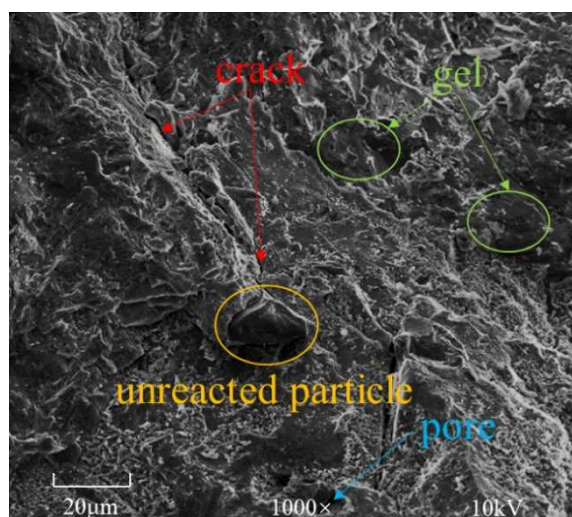
Figure 13. Microstructure of geopolymer

As shown in Figures 14a and 14b, the brick geopolymer had a cluster structure and a rough surface, indicating that the type of gel in brick geopolymer differed from that in other geopolymers. At 7 days of curing, brick geopolymer generated more gels but had more pores with a loose structure, resulting in low early strength. However, at 28 days of curing, the number of pores in the brick geopolymer decreased notably, leading to a high final strength. As illustrated in Figures 14c and 14d, the structure of ceramic geopolymer was highly uneven with numerous pores and cracks, and the gels were not completely bound together, resulting in low early strength. Although the number of large pores in ceramic geopolymer slightly improved from 7 to 28 days of curing, there were still many pores and cracks existing, which explained why the final strength remained low. The concrete geopolymer (Figures 14e and 14f) contained a large amount of gels and had a dense structure with no obvious pores or cracks, resulting in high strength. From 7 to 28 days of curing, the coating effect of the concrete geopolymer gel slightly improved, and no unreacted particles were detected.

The mixed precursor geopolymer (Figures 14g and 14h) also had a dense structure, leading to a relatively high strength. After 7 days of curing, there were more unreacted particles than the concrete. The consumption of alkaline activator by the concrete may adversely impact the dissolution of some brick and ceramic particles. From 7 to 28 days of curing, the number of unreacted particles decreased significantly as gels continued to form and coat these particles. Consequently, the strength of the mixed precursor geopolymer slightly improved in the later stage.

In sum, the microstructure of the mixed precursor geopolymer was the densest compared to the single component-derived geopolymers. The mixed precursor geopolymer had the highest strength, indicating that the strength of the geopolymer was closely related to the density of the structure. Although the microstructure of brick geopolymer was not dense, it formed clustered gels, which also remarkably influenced

516   the geopolymer strength. Therefore, it was deduced that both the type of gels and the
517   compactness of the structure significantly affected the strength of the geopolymer.
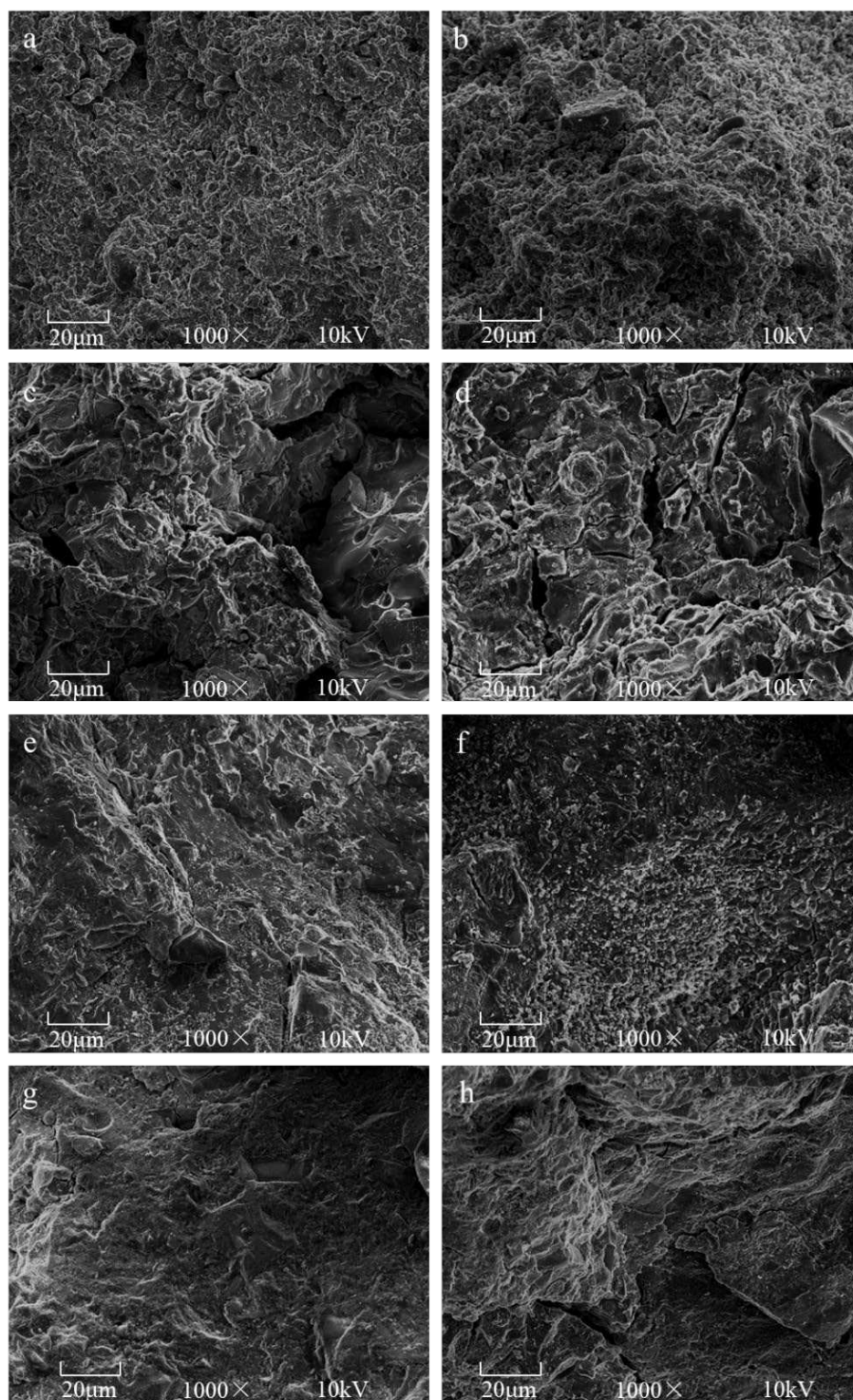
518
519   **Figure 14. SEM images of different brCDW based geopolymers at two curing**
520   **times: (a): 7d brick geopolymer, (b): 28d brick geopolymer, (c): 7d ceramic**
521   **geopolymer, (d): 28d ceramic geopolymer, (e): 7d concrete geopolymer, (f): 28d**
522   **concrete geopolymer, (g): 7d mixed precursor geopolymer, (h): 28d mixed**
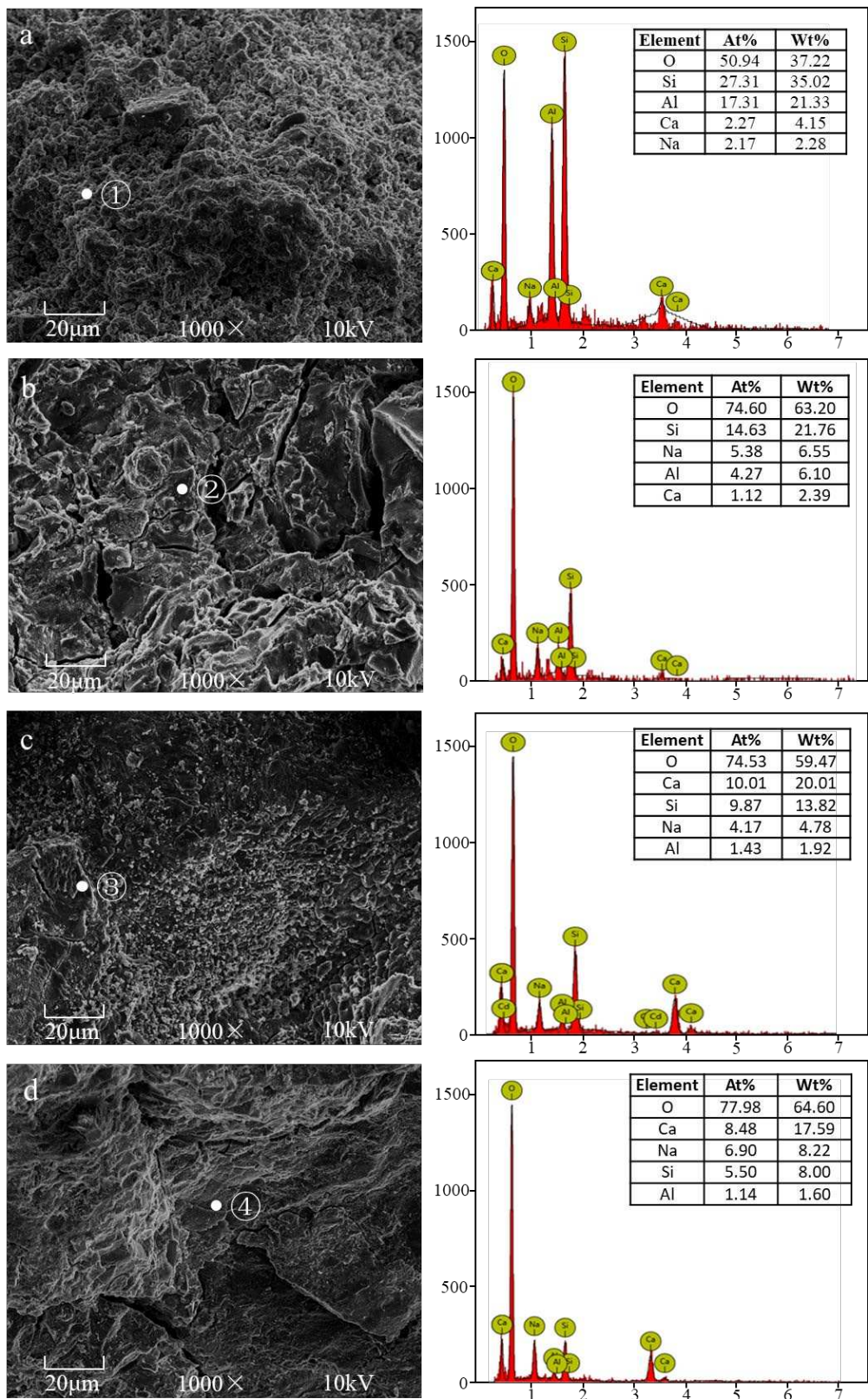523   **precursor geopolymer**

3.4.3 EDS test results

In addition to the SEM analysis, the EDS test was performed to determine the elemental composition of the gels. As shown in Figure 15a, the proportion sequences of the main elements in the gel of brick geopolymer were O, Si, Al, Ca, and Na. The elements of Si and Al had relatively high percentages, while the proportion of Ca was low, indicating a low probability of forming C-S-H and C-A-H gels. The likely gel types in the brick geopolymer were C-A-S-H and N-A-S-H gels, which coexisted to strength the material.

As presented in Figure 15b, the proportion sequences of the main elements in the gel of ceramic geopolymer were O, Si, Na, Al, and Ca. The Si element accounted for a relatively high proportion, while the Al element had a low proportion. Given the morphology of ceramic geopolymer, it was inferred that the amount of C-A-S-H and N-A-S-H gels formed in ceramic geopolymer was relatively small, and the major gel type was the C-S-H gel.

Figure 15c demonstrated that the proportion sequences of the main elements in the gel of concrete geopolymer were O, Ca, Si, Na, and Al. The elements of Ca and Si accounted for a relatively high proportion, while Al had a low proportion. This suggested that the gel type in concrete geopolymer was most likely to be the C-S-H gel. Additionally, the presence of Na and Al indicated that the gel might also contain an extremely low amount of C-A-S-H and N-A-S-H gels.

Figure 15d showed that the proportion sequences of the main elements in the gel of the mixed brCDW geopolymer were O, Ca, Na, Si, and Al. The elements of Ca, Na, and Si accounted for a relatively high proportion, while the Al element had a low proportion. Therefore, it was inferred that the dominant gel type in the mixed brCDW geopolymer was likely to be the C-S-H gel. Furthermore, the high proportion of Na and Ca suggested that the gel also contained the C-A-S-H and N-A-S-H gels.

Figure 15. SEM-EDS test results of different geopolymers after 28 days of curing: (a): brick geopolymer; (b): ceramic geopolymer; (c): concrete geopolymer; (d): mixed precursor geopolymer

556

4 Conclusions

In this study, the building-related construction and demolition waste (brCDW) was divided into three components, namely, brick, ceramic, and concrete. The influences of chemical composition and particle size of brCDW as precursors on the strength of the subsequent geopolymer were evaluated. The X-ray diffraction (XRD), scanning electron microscopy (SEM) and energy dispersive spectroscopy (EDS) tests were performed to investigate the strength evolution and mechanism of the single-component and mixed-component derived geopolymers. The major conclusions were summarized as follows.

- The brCDW components contained large amounts of Si, Al, and Ca elements, suggesting that the brCDW was a suitable precursor for synthesizing the geopolymer. Nonetheless, the chemical composition of each brCDW component differed, leading to differences in the strength of the resulting geopolymer. This indicated that the chemical composition of precursor material significantly affected the geopolymer strength. In addition, the strength of the geopolymer is significantly influenced by the modulus and dosage of the alkaline activator.

- The brick geopolymer exhibited a low strength in the early stage but a significantly high strength in the late stage. The ceramic geopolymer showed a low strength in both the early and late stages, indicating that it is not suitable for high-strength geopolymer production. The strength of concrete geopolymer was high in the early stage, but increased slowly later on. The strength evolution of the mixed brCDW geopolymer followed a similar pattern to that of the concrete geopolymer, as the mixed brCDW consisted of 79 % of concrete. The mixed brCDW geopolymer had the highest early strength and the second-highest final strength compared to the single component-derived geopolymers.

- The results of XRD, SEM and EDS analyses indicated that some precursor materials dissolved in the geopolymerization process, which then formed gels to coat and bind the unreacted particles and thereby resulting in a hardening strength. The formed gel type varied due to the different chemical composition ratios of each precursor material. The morphology and structure of brick geopolymer gels differed from other geopolymers, with the main gel products being C-A-S-H and N-A-S-H. The primary gel of ceramic, concrete, and mixed precursor geopolymers was the C-S-H gel, possibly with small amounts of C-A-S-H and N-A-S-H gel. Both the formed gel type and the compactness of the microstructure had significant influences on the geopolymer strength.

593

594

Credit authorship contribution statement

Fan Gu: Conceptualization, Methodology, Project Administration, Funding Acquisition, Writing-Drafting, Reviewing and Editing. **Jianwei Xie**: Methodology, Investigation, Writing-Original Draft. **Cedric Vuye**: Methodology, Funding acquisition, Writing-Reviewing and Editing. **Ya Wu**: Project administration, Funding acquisition, Writing-Reviewing and Editing. **Junhui Zhang**: Methodology, Project administration, Writing-Reviewing and Editing.

References

1. Ahmari, S., Ren, X., Toufigh, V., et al. (2012). Production of geopolymeric binder from blended waste concrete powder and fly ash. Construction and Building Materials, 35, 718-729.

2. Aiken, T. A., Kwasny, J., Sha, W., et al. (2018). Effect of slag content and activator dosage on the resistance of fly ash geopolymer binders to sulfuric acid attack. Cement and Concrete Research, 111, 23-40.

3. Akhtar, A., & Sarmah, A. K. (2018). Construction and demolition waste generation and properties of recycled aggregate concrete: A global perspective. Journal of Cleaner Production, 186, 262-281.

4. Aliques-Granero, J., Tognonvi, M. T., & Tagnit-Hamou, A. (2019). Durability study of AAMs: Sulfate attack resistance. Construction and Building Materials, 229, 117100.

5. Bai, G., Zhu, C., Liu, C., et al. (2020). An evaluation of the recycled aggregate characteristics and the recycled aggregate concrete mechanical properties. Construction and Building Materials, 240, 117978.

6. Barcelo, L., Kline, J., Walenta, G., et al. (2014). Cement and carbon emissions. Materials and structures, 47(6), 1055-1065.

7. Bassani, M., Tefa, L., Russo, A., et al. (2019). Alkali-activation of recycled construction and demolition waste aggregate with no added binder. Construction and Building Materials, 205, 398-413.

8. Chen, L., Wang, Z., Wang, Y., et al. (2016). Preparation and properties of alkali activated metakaolin-based geopolymer. Materials, 9(9), 767.

9. Chen, Z., Poon, C. S., Li, J. S., et al. (2021). Utilization of glass cullet to enhance the performance of recycled aggregate unbound sub-base. Journal of Cleaner Production, 288, 125083.

10. Davidovits, J. (1991). Geopolymers: inorganic polymeric new materials. Journal of Thermal Analysis and Calorimetry, 37(8), 1633-1656.

11. Feng, C., Cui, B., Huang, Y., et al. (2022). Enhancement technologies of recycled aggregate–Enhancement mechanism, influencing factors, improvement effects, technical difficulties, life cycle assessment. Construction and Building Materials, 317, 126168.

12. Gu, F., Ma, W., West, R. C., et al. (2019). Structural performance and sustainability assessment of cold central-plant and in-place recycled asphalt pavements: A case study. Journal of Cleaner Production, 208, 1513-1523.

13. Guo, H., Shi, C., Guan, X., et al. (2018). Durability of recycled aggregate concrete–A review. Cement and Concrete Composites, 89, 251-259.

14. Helmy, A. I. I. (2016). Intermittent curing of fly ash geopolymer mortar. Construction and Building Materials, 110, 54-64.

15. Hu, J., Liu, P., Huang, Q., et al. (2022). Research on interfacial zone failure of asphalt mixture mixed with recycled aggregates. Construction and Building Materials, 319, 126113.

16. Huo, W., Zhu, Z., Chen, W., et al. (2021). Effect of synthesis parameters on the development of unconfined compressive strength of recycled waste concrete powder-based geopolymers. Construction and Building Materials, 292, 123264.

17. Hwang, C. L., Yehualaw, M. D., Vo, D. H., et al. (2019). Performance evaluation of alkali activated mortar containing high volume of waste brick powder blended with ground granulated blast furnace slag cured at ambient temperature. Construction and Building Materials, 223, 657-667.

18. Jiang, X., Zhang, Y., Zhang, Y., et al. (2023). Influence of size effect on the properties of slag and waste glass-based geopolymer paste. Journal of Cleaner Production, 383, 135428.

19. Komnitsas, K., Zaharaki, D., & Perdikatsis, V. (2009). Effect of synthesis parameters on the compressive strength of low-calcium ferronickel slag inorganic polymers. Journal of Hazardous Materials, 161(2-3), 760-768.

20. Komnitsas, K., Zaharaki, D., Vlachou, A., et al. (2015). Effect of synthesis parameters on the quality of construction and demolition wastes (CDW) geopolymers. Advanced Powder Technology, 26(2), 368-376.

21. Kovtun, M., Kearsley, E. P., & Shekhovtsova, J. (2015). Dry powder alkali-activated slag cements. Advances in Cement Research, 27(8), 447-456.

22. Lahoti, M., Tan, K. H., & Yang, E. H. (2019). A critical review of geopolymer properties for structural fire-resistance applications. Construction and Building Materials, 221, 514-526.

23. Lemougna, P. N., Nzeukou, A., Aziwo, B., et al. (2020). Effect of slag on the improvement of setting time and compressive strength of low reactive volcanic ash geopolymers synthetized at room temperature. Materials Chemistry and Physics, 239, 122077.

24. Leong, H. Y., Ong, D. E. L., Sanjayan, J. G., et al. The effect of different Na2O and K2O ratios of alkali activator on compressive strength of fly ash based-geopolymer. Construction and Building Materials, 106, 500-511.

25. Li, L., Liu, Q., Huang, T., et al. Mineralization and utilization of CO2 in construction and demolition wastes recycling for building materials: A systematic review of recycled concrete aggregate and recycled hardened cement powder. Separation and Purification Technology, 121512.

26. Luna-Galiano, Y., Leiva, C., Arroyo, F., et al. (2022). Development of fly ash-based geopolymers using powder sodium silicate activator. Materials Letters, 320, 132346.

27. Luukkonen, T., Sreenivasan, H., Abdollahnejad, Z., et al. (2020). Influence of sodium silicate powder silica modulus for mechanical and chemical properties of dry-mix alkali-activated slag mortar. Construction and Building Materials, 233, 117354.

28. Ma, C., Zhao, B., Guo, S., et al. (2019). Properties and characterization of green one-part geopolymer activated by composite activators. Journal of Cleaner Production, 220, 188-199.

29. McLellan, B. C., Williams, R. P., Lay, J., et al. (2011). Costs and carbon emissions for geopolymer pastes in comparison to ordinary portland cement. Journal of Cleaner Production, 19(9-10), 1080-1090.

30. Mistri, A., Bhattacharyya, S. K., Dhami, N., et al. (2020). A review on different treatment methods for enhancing the properties of recycled aggregates for sustainable construction materials. Construction and Building Materials, 233, 117894.

31. Mohammed, M. S., ElKady, H., & Abdel-Gawwad, H. A. (2021). Utilization of construction and demolition waste and synthetic aggregates. Journal of Building Engineering, 43, 103207.

32. Moreno-Maroto, J. M., Delgado-Plana, P., Cabezas-Rodríguez, R., et al. (2022). Alkaline activation of high-crystalline low-Al2O3 Construction and Demolition Wastes to obtain geopolymers. Journal of Cleaner Production, 330, 129770.

33. Nie, Q., Hu, W., Huang, B., et al. (2019). Synergistic utilization of red mud for flue-gas desulfurization and fly ash-based geopolymer preparation. Journal of Hazardous Materials, 369, 503-511.

34. Ouyang, X., Ma, Y., Liu, Z., et al. (2019). Effect of the sodium silicate modulus and slag content on fresh and hardened properties of alkali-activated fly ash/slag. Minerals, 10(1), 15.

35. Özbayrak, A., Kucukgoncu, H., Aslanbay, H. H., et al. (2023). Comprehensive experimental analysis of the effects of elevated temperatures in geopolymer concretes with variable alkali activator ratios. Journal of Building Engineering, 68, 106108.

36. Patil, A. A., Chore, H. S., & Dode, P. A. (2014). Effect of curing condition on strength of geopolymer concrete. Advances in Concrete Construction, 2(1), 029.

37. Peng, X., Shi, F., Yang, J., et al. (2023). Modification of construction waste derived recycled aggregate via CO2 curing to enhance corrosive freeze-thaw durability of concrete. Journal of Cleaner Production, 405, 137016.

38. Petrakis, E., Karmali, V., Bartzas, G., et al. (2019). Grinding kinetics of slag and effect of final particle size on the compressive strength of alkali activated materials. Minerals, 9(11), 714.

39. Shill, S. K., Al-Deen, S., Ashraf, M., et al. (2020). Resistance of fly ash based geopolymer mortar to both chemicals and high thermal cycles simultaneously. Construction and Building Materials, 239, 117886.

40. Sivasakthi, M., & Jeyalakshmi, R. (2021). Effect of change in the silica modulus of sodium silicate solution on the microstructure of fly ash geopolymers. Journal of Building Engineering, 44, 102939.

41. Sun, Z., Cui, H., An, H., et al. (2013). Synthesis and thermal behavior of geopolymer-type material from waste ceramic. Construction and Building Materials, 49, 281-287.

42. Tan, J., Cai, J., & Li, J. (2022). Recycling of unseparated construction and demolition waste (UCDW) through geopolymer technology. Construction and Building Materials, 341, 127771.

43. Tang, Q., Tian, A., Ling, C., et al. (2023). Physical and mechanical properties of recycled aggregates modified by microbially induced calcium carbonate precipitation. Journal of Cleaner Production, 382, 135409.

44. Tang, Q., Xiao, P., Kou, C., et al. (2021). Physical, chemical and interfacial properties of modified recycled concrete aggregates for asphalt mixtures: A review. Construction and Building Materials, 312, 125357.

45. Tchakouté, H. K., Rüscher, C. H., Kong, S., et al. (2017). Thermal behavior of metakaolin-based geopolymer cements using sodium waterglass from rice husk ash and waste glass as alternative activators. Waste and Biomass Valorization, 8, 573-584.

46. Temuujin, J., van Riessen, A., & MacKenzie, K. J. D. (2010). Preparation and characterisation of fly ash based geopolymer mortars. Construction and Building Materials, 24(10), 1906-1910.

47. Tuyan, M., Andiç-Çakir, Ö., & Ramyar, K. (2018). Effect of alkali activator concentration and curing condition on strength and microstructure of waste clay brick powder-based geopolymer. Composites Part B: Engineering, 135, 242-252.

48. Vafaei, M., Allahverdi, A., Dong, P., et al. (2018). Acid attack on geopolymer cement mortar based on waste-glass powder and calcium aluminate cement at mild concentration. Construction and Building Materials, 193, 363-372.

49. Yang, Z., Mocadlo, R., Zhao, M., et al. (2019). Preparation of a geopolymer from red mud slurry and class F fly ash and its behavior at elevated temperatures. Construction and Building Materials, 221, 308-317.

50. Zhang, J., Ding, L., Li, F., et al. (2020). Recycled aggregates from construction and demolition wastes as alternative filling materials for highway subgrades in China. Journal of Cleaner Production, 255, 120223.

51. Zhang, J., Gu, F., & Zhang, Y. (2019). Use of building-related construction and demolition wastes in highway embankment: laboratory and field evaluations. Journal of Cleaner production, 230, 1051-1060.

52. Zhang, J., Li, S., Li, Z., et al. (2020). Feasibility study of red mud for geopolymer preparation: effect of particle size fraction. Journal of Material Cycles and Waste Management, 22, 1328-1338.

53. Zhang, P., Gao, Z., Wang, J., et al. (2020). Properties of fresh and hardened fly ash/slag based geopolymer concrete: A review. Journal of Cleaner Production, 270, 122389.

54. Jiang, X., Zhang, Y., Zhang, Y., et al. (2023). Influence of size effect on the properties of slag and waste glass-based geopolymer paste. Journal of Cleaner Production, 383, 135428.

55. Xiao, R., Huang, B., Zhou, H., et al. (2022). A state-of-the-art review of crushed urban waste glass used in OPC and AAMs (geopolymer): Progress and challenges. Cleaner Materials, 4, 100083.

56. Zhang, Y., Xiao, R., Jiang, X., et al. (2020). Effect of particle size and curing temperature on mechanical and microstructural properties of waste glass-slag-based and waste glass-fly ash-based geopolymers. Journal of Cleaner Production, 273, 122970.

57. Obeng, J., Andrews, A., Adom-Asamoah, M., et al. (2023). Effect of calcium carbide residue on the sulphate resistance of metakaolin-based geopolymer mortars. Cleaner Materials, 7, 100177.

58. Gill, P., Jangra, P., Roychand, R., et al. (2023). Effects of various additives on the crumb rubber integrated geopolymer concrete. Cleaner Materials, 8, 100181.

59. Neupane, K. (2022). Evaluation of environmental sustainability of one-part geopolymer binder concrete. Cleaner Materials, 6, 100138.